Synthesis of 2-Layers Ogive Radome through a Surrogate Assisted Method

M. Salucci, G. Oliveri, M. A. Hannan and A. Massa

Contents

1 Fitness definition **3**

2 Geometry and optimization parameters **4**

3 Synthesis of a 2-Layer Ogive Radome **5**

3.1 Selecting the proper correlation model 5

3.2 Optimization 11

1 Fitness definition

The fitness (cost function) associated to the trial individual $\mathbf{x}$ is defined as

$$\Phi(\mathbf{x}) = \frac{1}{N_f}\sum_{n=1}^{N_f}\frac{\int_{\theta_{min}}^{\theta_{max}}\int_{\phi_{min}}^{\phi_{max}}\left|\left|\mathbf{E}^{FS}(\theta,\phi,f_n)\right|-\left|\mathbf{E}^{RAD}(\theta,\phi,f_n,\mathbf{x})\right|\right|^2 d\phi\, d\theta}{\int_{\theta_{min}}^{\theta_{max}}\int_{\phi_{min}}^{\phi_{max}}\left|\mathbf{E}^{FS}(\theta,\phi,f_n)\right|^2 d\phi\, d\theta} \quad (1)$$

where

- N_f is the number of frequency steps
- $\mathbf{E}^{FS}$ is the field radiated by the antenna in free space
- $\mathbf{E}^{RAD}$ is the field radiated by the antenna enclosed into the radome
- $\theta \in [\theta_{min}, \theta_{max}]$, $\phi \in [\phi_{min}, \phi_{max}]$ are the angular coordinates.

2 Geometry and optimization parameters

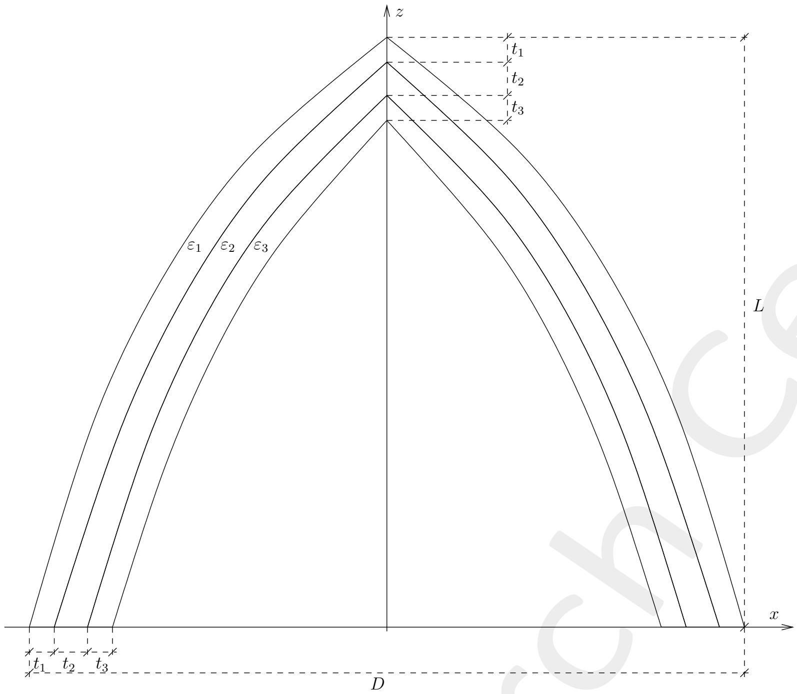

Figure 1: Geometry of the ogive radome.

Parameter	Description
$t_n,\ n = 1, ..., N$	Thickness of the n-th radome layer
$\varepsilon_n, n = 1, ..., N$	Permittivity of the n-th radome layer

Table I: List of the optimization parameters

3 Synthesis of a 2-Layer Ogive Radome

3.1 Selecting the proper correlation model

Kriging (Gaussian Process Regressor) parameters

- Regression model: constant (Ordinary Kriging);
- Correlation models:
  - Exponential ($p = 1$);
  - Gaussian ($p = 2$);
- Initial guess for hyper-parameters θ_h: $\theta_{h,0} = 0.5$, for $h = 1, ..., K$;
- Lower bound for hyper-parameters θ_h: $min\left\{\theta_h\right\} = 0.1$, for $h = 1, ..., K$;
- Upper bound for hyper-parameters θ_h: $max\left\{\theta_h\right\} = 20.0$, for $h = 1, ..., K$;

Incremental training parameters

- Number of available simulations: $S = 2000$ (LHS sampling);
- Dimension of the training sets: $N_1 = 50$, $N_{max} = N_L = 1500$, step $\Delta N = 50$;

Predicted Fitness Values

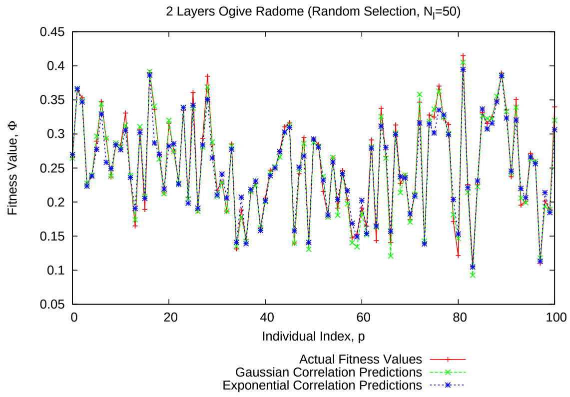

(a) $N = 50$

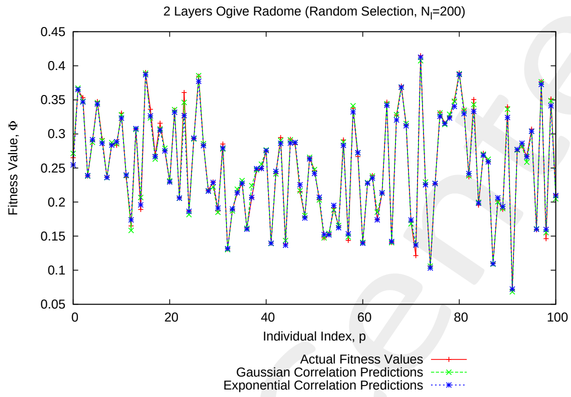

(b) $N = 200$

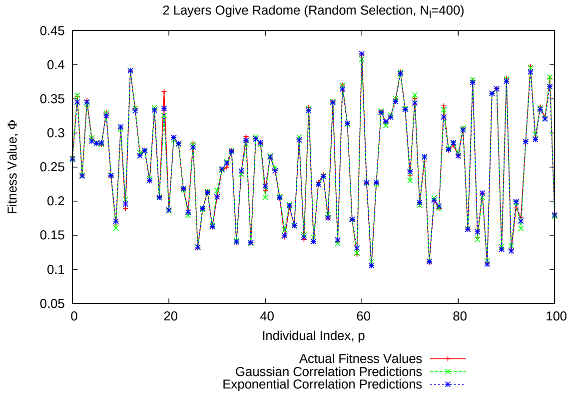

(c) $N = 400$

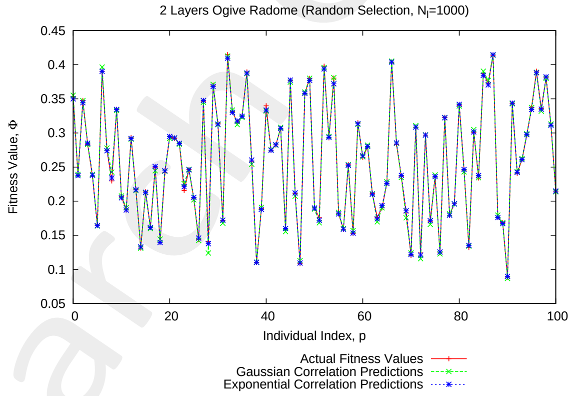

(d) $N = 1000$

Figure 2: *(2-layer ogive radome optimization)* – Actual and predicted functional values of 100 random individuals for different training sizes (N): (a) $N = 50$, (b) $N = 200$, (c) $N = 400$ and (d) $N = 1000$.

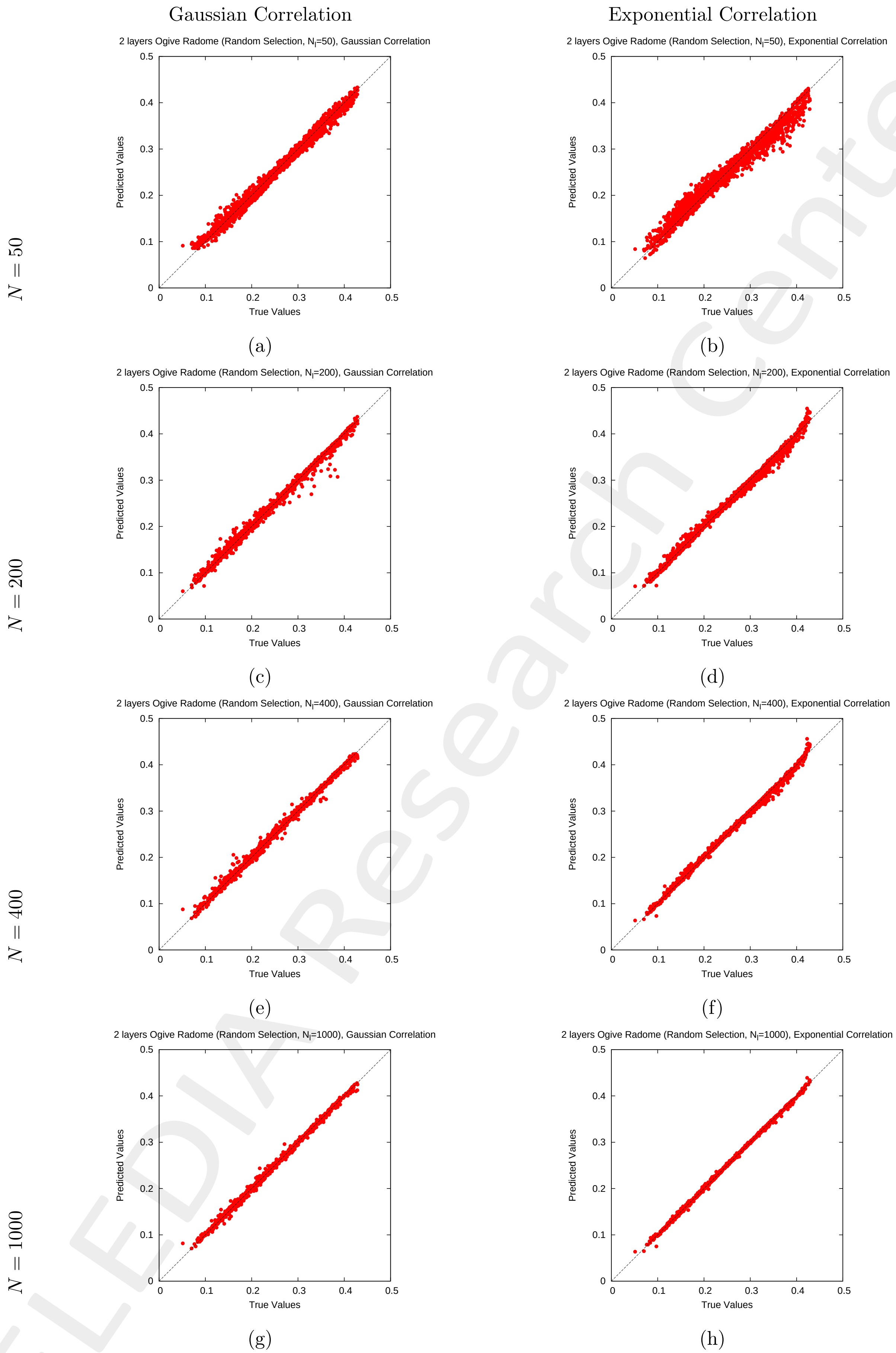

Figure 3: *(3-layer ogive radome optimization)* – Plot of predicted vs actual values for (a), (c), (e), (g) Gaussian Correlation Model and (b), (d), (f), (h) Exponential Correlation Model for different training sizes (N): (a),(b) $N = 50$, (c),(d) $N = 200$, (e),(f) $N = 400$ and (g),(h) $N = 1000$.

Prediction Error vs Training Size

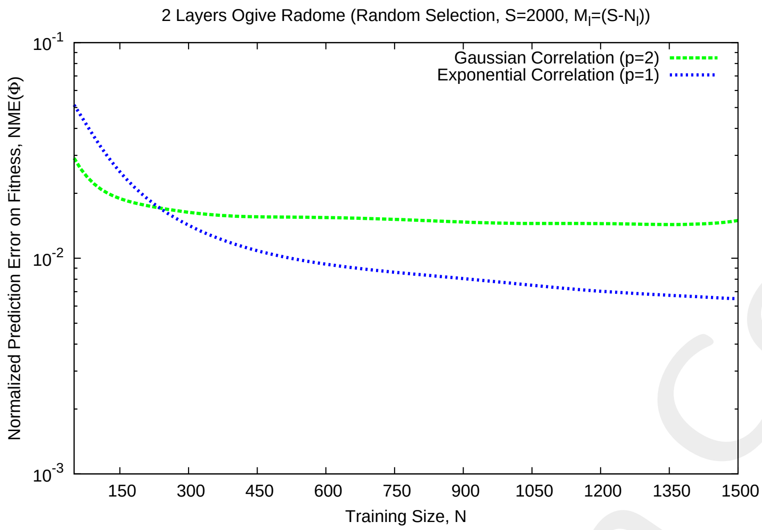

(a) NME

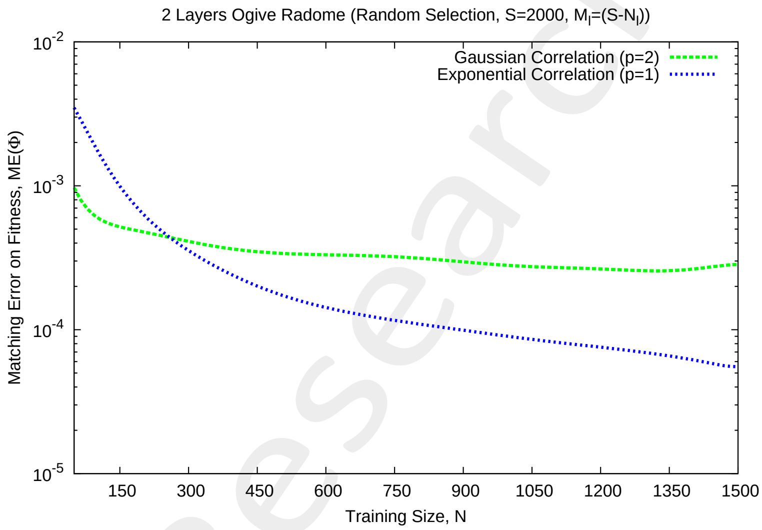

(b) ME

Figure 4: *(2-layer ogive radome optimization)* – Plot of (a) Normalized Mean Error (NME) and (b) Matching Error (ME) vs training size (N) when considering an incremental training with random selection of N_l training samples form a set of S available simulations and testing the corresponding Kriging model on a test set made by the remaining $M_l = (S - N_l)$ simulations.

	Gaussian Correlation		Exponential Correlation	
N	NME	ME	NME	ME
50	2.91×10^{-2}	9.70×10^{-4}	5.14×10^{-2}	3.49×10^{-3}
200	1.77×10^{-2}	6.16×10^{-4}	1.82×10^{-2}	5.52×10^{-4}
400	1.53×10^{-2}	3.67×10^{-4}	1.11×10^{-2}	2.39×10^{-4}
1000	1.45×10^{-2}	2.65×10^{-4}	7.82×10^{-3}	8.76×10^{-5}

Table II: *(3 layer ogive radome optimization)* – Normalized Mean Error (NME) and Matching Error (ME) vs training size (N).

Time Saving Analysis

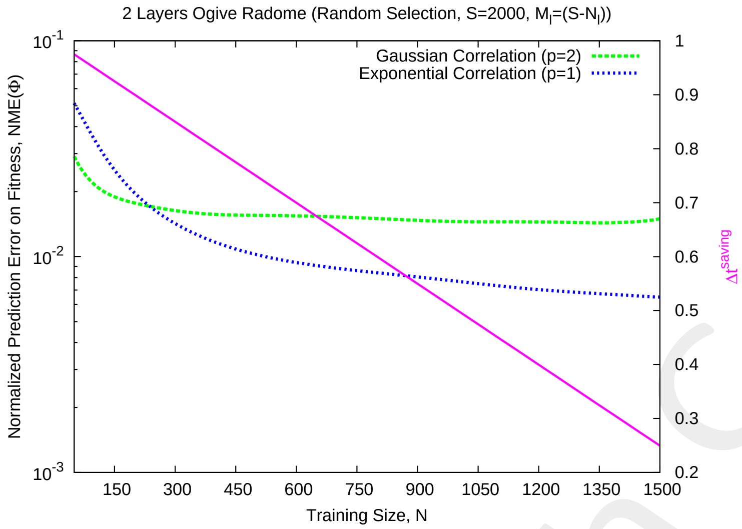

(a) NME

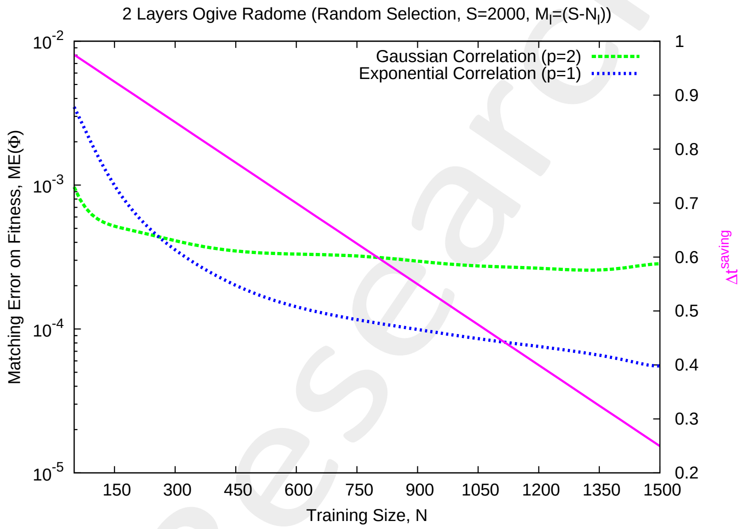

(b) ME

Figure 5: *(2-layer ogive radome optimization)* – Plot of Time Saving (Δt^{saving}) with (a) Normalized Mean Error (NME) and (b) Matching Error (ME) vs training size (N) when considering an incremental training with random selection of N_l training samples form a set of S available simulations and testing the corresponding Kriging model on a test set made by the remaining $M_l = (S - N_l)$ simulations.

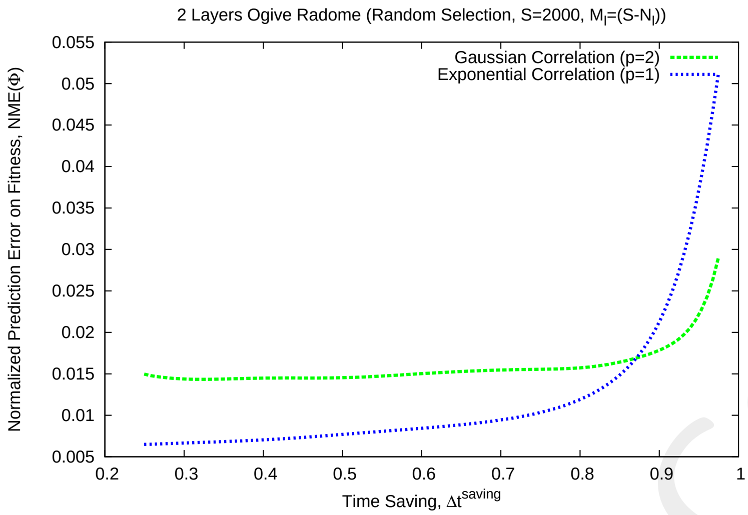

(a) NME

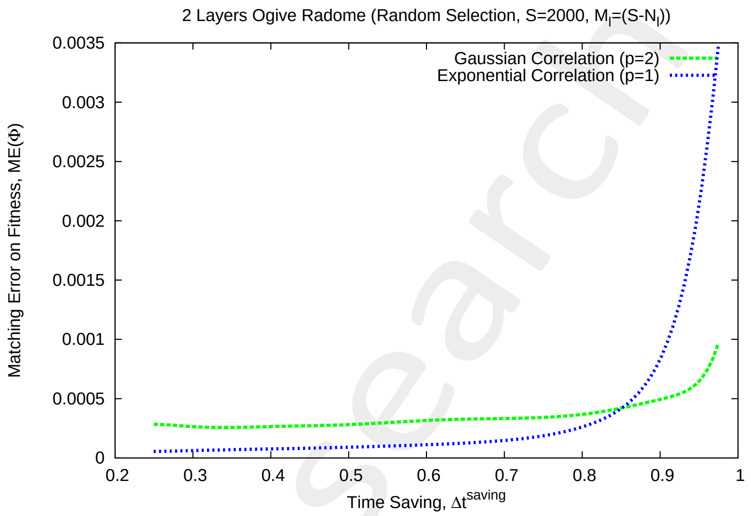

(b) ME

Figure 6: *(2-layer ogive radome optimization)* – Plot of (a) Normalized Mean Error (NME) and (b) Matching Error (ME) vs Time Saving (Δt^{saving}).

3.2 Optimization

Parameters

Optimization targets

- Functional dimension: $J = 1$;
- Target frequencies:
  1. $f_1 = 200.0$ [MHz];

$SADE$ **parameters**

- Number of variables: $K = 4$;
- Population dimension: $P = 20$;
- Scaling factor: $Q = 0.6$;
- Crossover probability: $P_c = 0.8$;
- Primary parent selection mode: $SADE/RAND/1$;
- Maximum number of iterations: $I = 1000$;
- Fitness threshold: $\Phi^{th} = 10^{-20}$;
- Dimension of the training set: $\tau = 100$;
- Initialization strategy: ELEDIA (random P individuals + $(\tau - P)$ generated via LHS);
- Pre-screening strategy: LCB, $\omega = 2$;
- Update strategy: most promising individual overwrites itself;
- Random seed: $S = 1$;

Kriging (Gaussian Process Regressor) parameters

- Regression model: constant (Ordinary Kriging);
- Correlation models:
  - Exponential ($p = 1$);
  - Gaussian ($p = 2$);
- Initial guess for hyper-parameters θ_h: $\theta_{h,0} = 0.5$, for $h = 1, ..., K$;
- Lower bound for hyper-parameters θ_h: $min\left\{\theta_h\right\} = 0.1$, for $h = 1, ..., K$;

* Upper bound for hyper-parameters θ_h: $max\{\theta_h\} = 20.0$, for $h = 1, ..., K$;

Not-optimized (static) radome parameters

* Radome length: $L = 1.75\ [m] \simeq 1.17\lambda$;
* Radome base diameter: $D = 1.6\ [m] \simeq 1.07\lambda$;
* Curvature type: $\nu = 1.449$ (tangent ogive);
* Loss tangent of the layers: $tan\delta = 0.00$;

Antenna Parameters

* Dipole centered in $(x, y, x) = (0, 0, 0)$ and directed along $\hat{\mathbf{y}}$;
* Dipole length: $l_d = 0.75\ [m] = \frac{\lambda}{2}$;

Optimized parameters boundaries

Parameter	Description	Min	Max	Measure unit
ε_1	Relative permittivity of the layer 1	3.00	6.00	//
ε_2	Relative permittivity of the layer 2	3.00	6.00	//
t_1	Thickness of the layer 1	1.00×10^{-2}	5.00×10^{-2}	[m]
t_2	Thickness of the layer 2	1.00×10^{-2}	5.00×10^{-2}	[m]

Table III: *(2-layer ogive radome optimization)* – List of all considered boundaries for the optimized radome descriptors.

Results of the optimization

- Number of performed $SADE$ iterations: $I_{tot} = I = 1000$;
- Final value of the fitness:
  - Gaussian correlation: $\Phi^{(i=I_{tot})} = 2.92 \times 10^{-2}$;
  - Exponential correlation: $\Phi^{(i=I_{tot})} = 1.89 \times 10^{-2}$;
- Total number of $FEKO$ simulations: $E = (\tau + I_{tot}) = 100 + 1000 = 1100$;

Computational time (@eledialab22-Intel(R) Core(TM) i5 CPU 650 @ 3.20GHz, 4-GB-Ram)

- Average time to compute the fitness associated to a trial solution (**1 core-simulation**): $\Delta t_{avg}^{sim} \simeq 160$ [sec];
- Time for training a Kriging surrogate model with $\tau = 100$ $K = 4$-dimensional training samples: $\Delta t^{train}\big|_{N=\tau=100} \simeq 0.1$ [sec];
- Time for testing $P = 20$ $K = 4$-dimensional trial solutions using a Kriging surrogate model (built on $\tau = 100$ training samples): $\Delta t^{test}|_{M=P=20} \simeq 0.03$ [sec];
- Real total duration of the optimization: $\Delta t^{tot} \simeq 48$ [hours].

Fitness

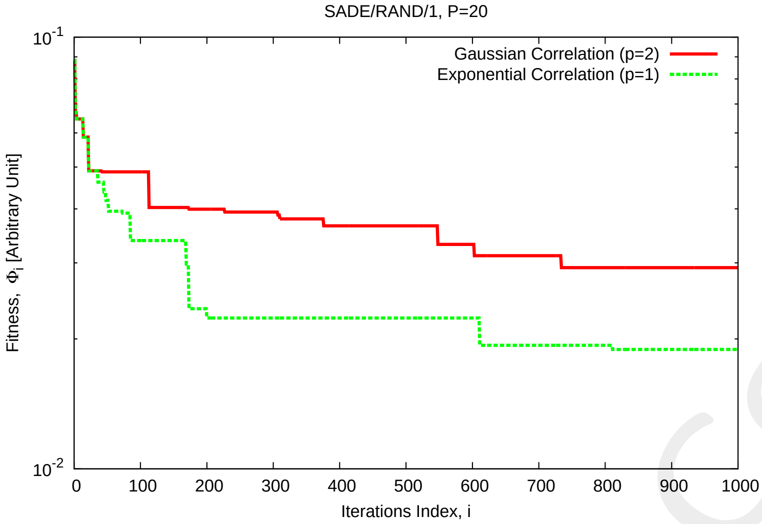

(a)

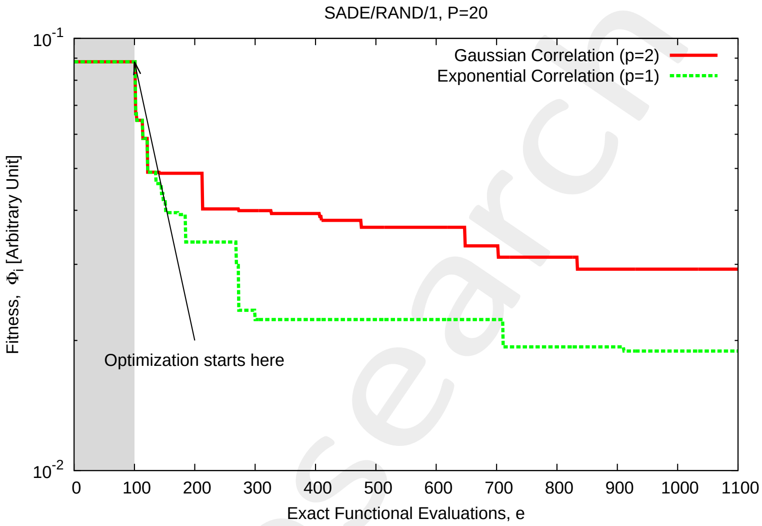

(b)

Figure 7: *(2-layer ogive radome optimization)* – Total fitness evolution; (a) evolution vs iteration index during the SADE optimization; (b) evolution vs number of exact function evaluations.

Comparison: $SADE/RAND/1$ **vs** $DE/RAND/1$

The same optimization (i.e., by using the same parameters, such as the random seed and, thus, forcing the same initial population) has been executed using a classic Differential Evolution (DE) algorithm. In particular, the following parameters have been set for DE:

- Population dimension: $P = 20$;
- Scaling factor: $Q = 0.6$;
- Crossover probability: $P_c = 0.8$;
- Primary parent selection mode: $DE/RAND/1$;
- Maximum number of iterations: $I = 1000$;
- Fitness threshold: $\Phi^{th} = 10^{-20}$;
- Random seed: $S = 1$ (same initial population).

Fitness

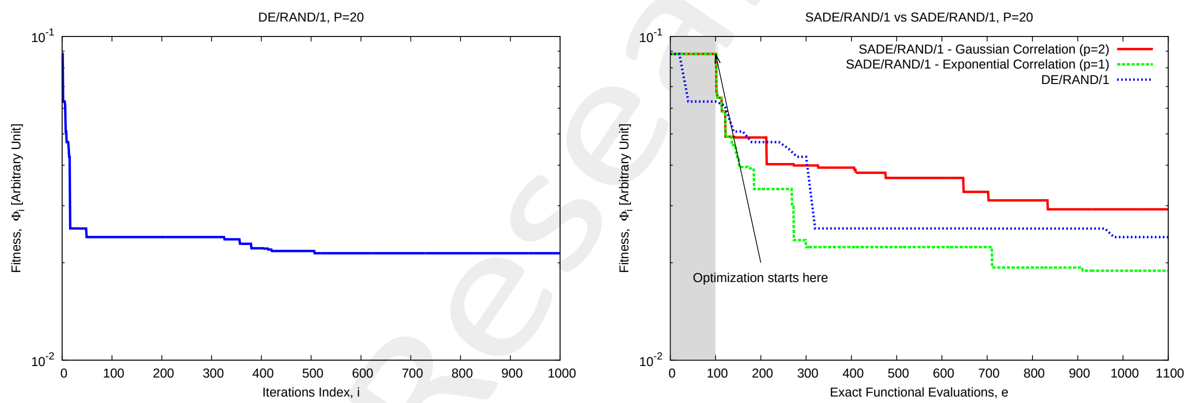

(a) (b)

Figure 8: Total fitness evolution; (a) evolution vs iteration index during the DE optimization; (b) evolution vs number of exact function evaluations (simulations with $FEKO$) for both $SADE/RAND/1$ and $DE/RAND/1$ executions.

Computational time

- Theoretical total duration of the optimization:
  - $SADE$ algorithm ($\tau = 100,\ I_{tot} = 1000$):
    $\Delta t^{tot}_{SADE} \simeq \tau \times \Delta t^{\Phi}_{avg} + I_{tot} \times \left(\Delta t^{train}\big|_{N=\tau=200} + \Delta t^{test}\big|_{M=P=20} + \Delta t^{\Phi}_{avg}\right) \simeq 49$ [hours];
  - DE algorithm ($I_{tot} = 1000,\ P = 20$):
    $\Delta t^{tot}_{DE} \simeq I_{tot} \times P \times \Delta t^{\Phi}_{avg} \simeq 890$ [hours] ($\simeq 37$ [days]);

Evolution of the simulated individuals stored inside the database

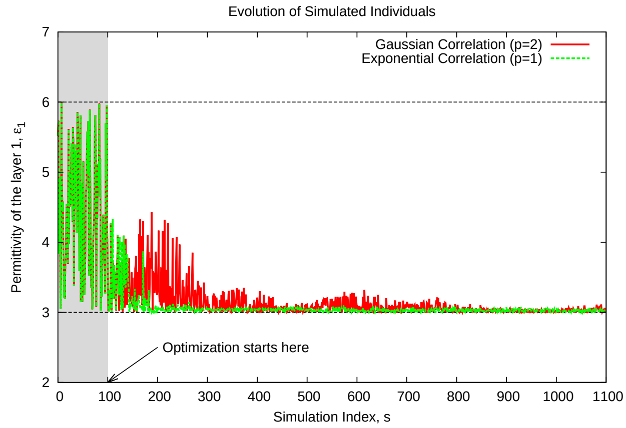

(a)

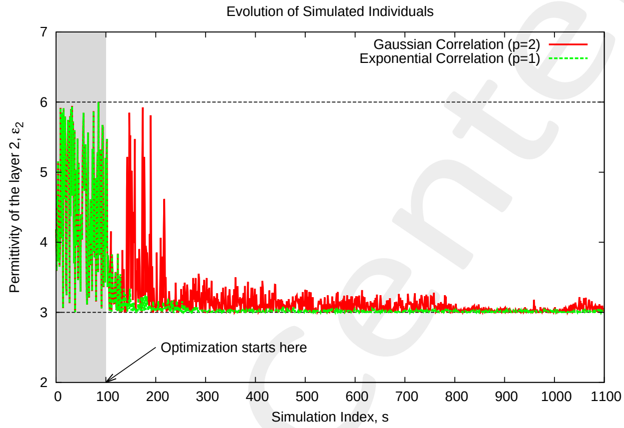

(b)

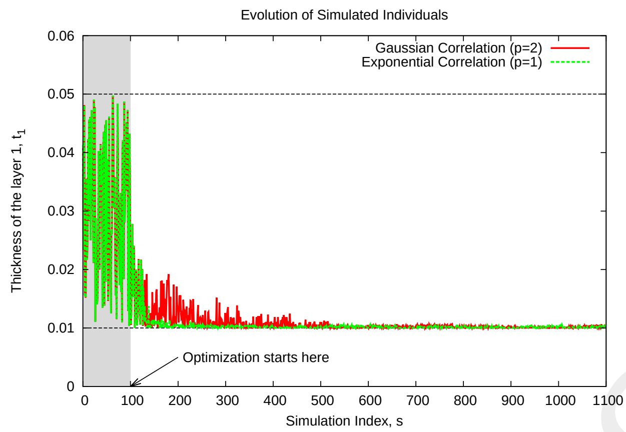

(c)

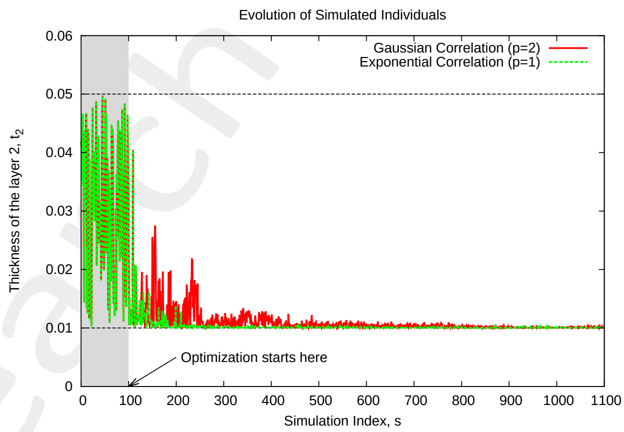

(d)

Figure 9: *(2-layer ogive radome optimization)* – Evolution of simulated individuals stored inside the database: parameter (a) ε_1, (b) ε_2, (c) t_1 and (d) t_2.

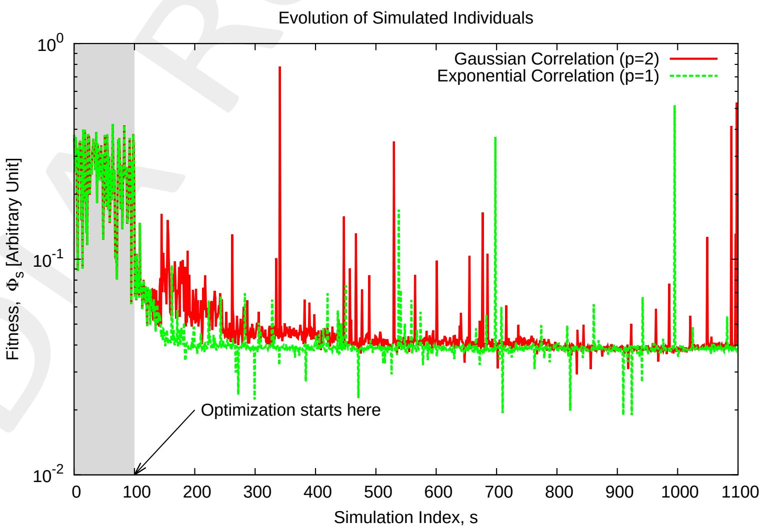

Figure 10: *(2-layer ogive radome optimization)* – Evolution of the fitness of the individuals stored inside the database.

Analysis of the optimal individual

Optimized Model

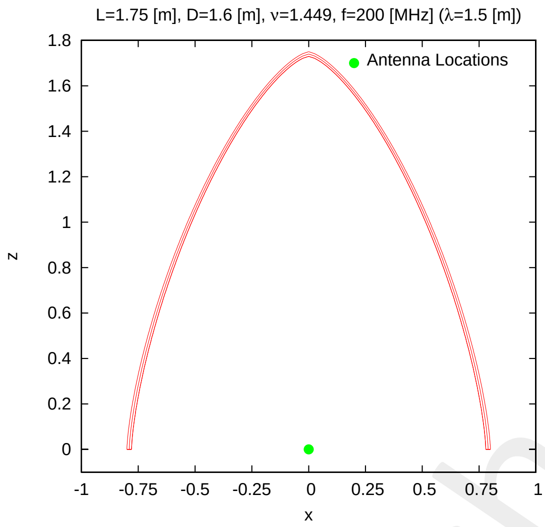

(a)

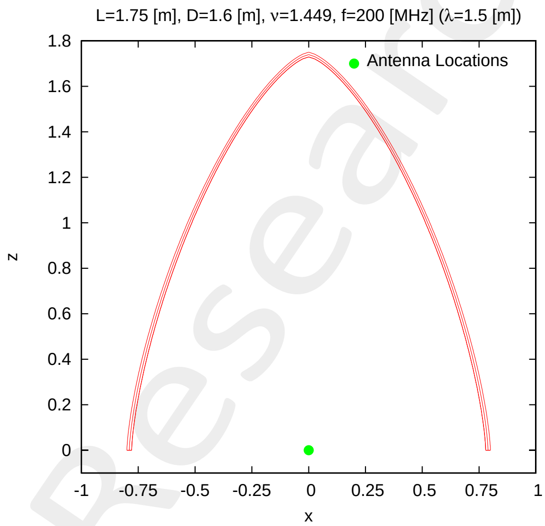

(b)

Figure 11: *(2-layer ogive radome optimization)* – Geometry of the optimized radome: (a) Gaussian correlation solution and (b) Exponential correlation solution.

- Total thickness of the structure:
  - Gaussian Correlation: $t = t_1 + t_2 \simeq 2.05 \times 10^{-2}$ $[m]$
  - Exponential Correlation: $t = t_1 + t_2 \simeq 2.02 \times 10^{-2}$ $[m]$

Parameter	Description	Value - Gauss. Corr. $(p = 2)$	Value - Exp. Corr. $(p = 1)$
ε_1	Relative permittivity of the layer 1	3.02	3.02
ε_2	Relative permittivity of the layer 2	3.05	3.00
t_1	Thickness of the layer 1	1.03×10^{-2} [m]	1.01×10^{-2} [m]
t_2	Thickness of the layer 2	1.02×10^{-2} [m]	1.01×10^{-2} [m]

Table IV: *(2-layer ogive radome optimization)* – Optimized values for all considered radome descriptors.

Radiation Diagrams

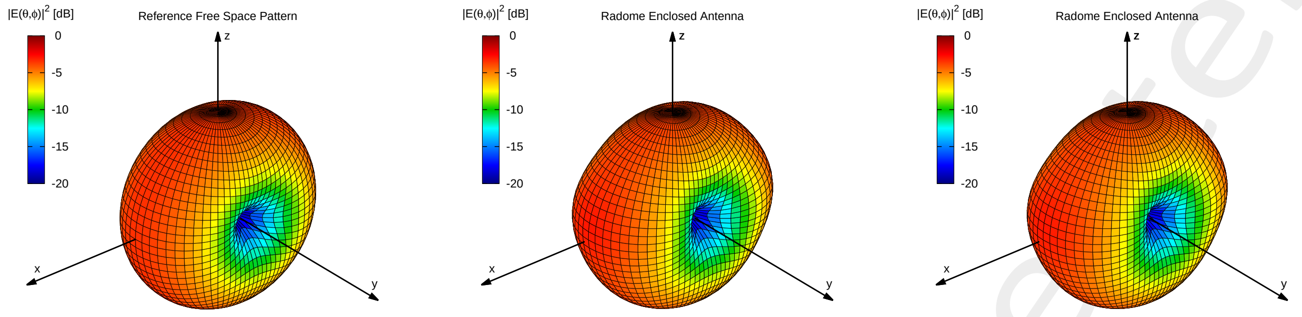

(a) (b) (c)

Figure 12: *(2-layer ogive radome optimization)* – 3D plot of the power pattern of (a) the antenna in free-space, (b) the antenna enclosed in the optimized radome (Gaussian Correlation solution) and (c) the antenna enclosed in the optimized radome (Exponential Correlation solution).

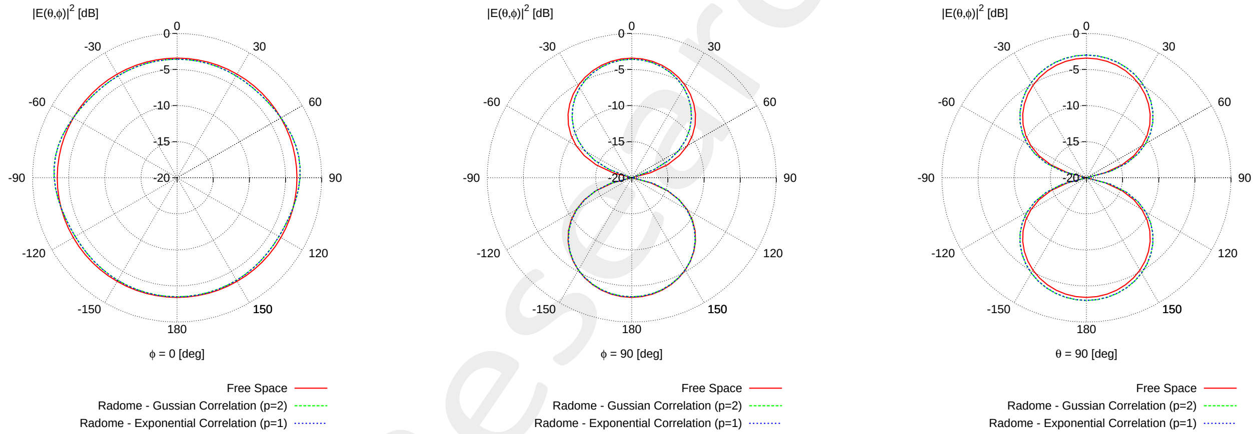

(a) (b) (c)

Figure 13: *(2-layer ogive radome optimization)* – Polar plot of the power pattern of the antenna in free space and in presence of the radome (Gaussian and Exponential Correlation solutions): (a) $\phi = 0$ $[deg]$ plane, (b) $\phi = 90$ $[deg]$ plane and (c) $\theta = 0$ $[deg]$ plane.

More information on the topics of this document can be found in the following list of references.

References

[1] A. Massa, D. Marcantonio, X. Chen, M. Li, and M. Salucci, "DNNs as applied to electromagnetics, antennas, and propagation - A review," *IEEE Antennas and Wirel. Propag. Lett.,* vol. 18, no. 11, pp. 2225-2229, Nov. 2019.

[2] A. Massa, G. Oliveri, M. Salucci, N. Anselmi, and P. Rocca, "Learning-by-examples techniques as applied to electromagnetics," *Journal of Electromagnetic Waves and Applications, Invited Review Article*, pp. 1-16, 2017.

[3] G. Oliveri, M. Salucci, and A. Massa, "Towards reflectarray digital twins - An EM-driven machine learning perspective," *IEEE Trans. Antennas Propag. - Special Issue on 'Machine Learning in Antenna Design, Modeling, and Measurements*', vol. 70, no. 7, pp. 5078-5093, July 2022.

[4] M. Salucci, L. Tenuti, G. Oliveri, and A. Massa, "Efficient prediction of the EM response of reflectarray antenna elements by an advanced statistical learning method," *IEEE Trans. Antennas Propag.*, vol. 66, no. 8, pp. 3995-4007, Aug. 2018.

[5] M. Salucci, G. Oliveri, M. A. Hannan, and A. Massa, "System-by-design paradigm-based synthesis of complex systems: The case of spline-contoured 3D radomes," *IEEE Antennas and Propagation Magazine - Special Issue on 'Artificial Intelligence in Electromagnetics,*', vol. 64, no. 1, pp. 72-83, Feb. 2022.

[6] G. Oliveri, P. Rocca, M. Salucci, and A. Massa, "Holographic smart EM skins for advanced beam power shaping in next generation wireless environments," *IEEE J. Multiscale Multiphysics Comput. Tech.*, vol. 6, pp. 171-182, Oct. 2021.

[7] G. Oliveri, A. Gelmini, A. Polo, N. Anselmi, and A. Massa, "System-by-design multi-scale synthesis of task-oriented reflectarrays," *IEEE Trans. Antennas Propag.*, vol. 68, no. 4, pp. 2867-2882, Apr. 2020.

[8] M. Salucci, L. Tenuti, G. Gottardi, A. Hannan, and A. Massa, "System-by-design method for efficient linear array miniaturisation through low-complexity isotropic lenses" *Electronic Letters*, vol. 55, no. 8, pp. 433-434, May 2019.

[9] M. Salucci, N. Anselmi, S. Goudos, and A. Massa, "Fast design of multiband fractal antennas through a system-by-design approach for NB-IoT applications," *EURASIP J. Wirel. Commun. Netw.*, vol. 2019, no. 1, pp. 68-83, Mar. 2019.

[10] M. Salucci, G. Oliveri, N. Anselmi, and A. Massa, "Material-by-design synthesis of conformal miniaturized linear phased arrays," *IEEE Access*, vol. 6, pp. 26367-26382, 2018.

[11] M. Salucci, G. Oliveri, N. Anselmi, G. Gottardi, and A. Massa, "Performance enhancement of linear active electronically-scanned arrays by means of MbD-synthesized metalenses," *Journal of Electromagnetic Waves and Applications*, vol. 32, no. 8, pp. 927-955, 2018.

[12] G. Oliveri, M. Salucci, N. Anselmi and A. Massa, "Multiscale System-by-Design synthesis of printed WAIMs for waveguide array enhancement," *IEEE J. Multiscale Multiphysics Computat. Techn.*, vol. 2, pp. 84-96, 2017.

[13] A. Massa and G. Oliveri, "Metamaterial-by-Design: Theory, methods, and applications to communications and sensing - Editorial," *EPJ Applied Metamaterials*, vol. 3, no. E1, pp. 1-3, 2016.

[14] G. Oliveri, F. Viani, N. Anselmi, and A. Massa, "Synthesis of multi-layer WAIM coatings for planar phased arrays within the system-by-design framework," *IEEE Trans. Antennas Propag.*, vol. 63, no. 6, pp. 2482-2496, June 2015.

[15] G. Oliveri, L. Tenuti, E. Bekele, M. Carlin, and A. Massa, "An SbD-QCTO approach to the synthesis of isotropic metamaterial lenses" *IEEE Antennas Wireless Propag. Lett.*, vol. 13, pp. 1783-1786, 2014.

[16] A. Massa, G. Oliveri, P. Rocca, and F. Viani, "System-by-Design: a new paradigm for handling design complexity," *8th European Conference on Antennas Propag. (EuCAP 2014), The Hague, The Netherlands*, pp. 1180-1183, Apr. 6-11, 2014.

[17] P. Rocca, M. Benedetti, M. Donelli, D. Franceschini, and A. Massa, "Evolutionary optimization as applied to inverse problems," *Inverse Problems - 25 th Year Special Issue of Inverse Problems, Invited Topical Review*, vol. 25, pp. 1-41, Dec. 2009.

[18] P. Rocca, G. Oliveri, and A. Massa, "Differential Evolution as applied to electromagnetics," *IEEE Antennas Propag. Mag.*, vol. 53, no. 1, pp. 38-49, Feb. 2011.

[19] P. Rocca, N. Anselmi, A. Polo, and A. Massa, "Pareto-optimal domino-tiling of orthogonal polygon phased arrays," *IEEE Trans. Antennas Propag.*, vol. 70, no. 5, pp. 3329-3342, May 2022.

[20] P. Rocca, N. Anselmi, A. Polo, and A. Massa, "An irregular two-sizes square tiling method for the design of isophoric phased arrays," *IEEE Trans. Antennas Propag.*, vol. 68, no. 6, pp. 4437-4449, Jun. 2020.

[21] P. Rocca, N. Anselmi, A. Polo, and A. Massa, "Modular design of hexagonal phased arrays through diamond tiles," *IEEE Trans. Antennas Propag.*, vol.68, no. 5, pp. 3598-3612, May 2020.

[22] N. Anselmi, L. Poli, P. Rocca, and A. Massa, "Design of simplified array layouts for preliminary experimental testing and validation of large AESAs," *IEEE Trans. Antennas Propag.*, vol. 66, no. 12, pp. 6906-6920, Dec. 2018.

[23] N. Anselmi, P. Rocca, M. Salucci, and A. Massa, "Contiguous phase-clustering in multibeam-on-receive scanning arrays," *IEEE Trans. Antennas Propag.*, vol. 66, no. 11, pp. 5879-5891, Nov. 2018.

[24] G. Oliveri, G. Gottardi, F. Robol, A. Polo, L. Poli, M. Salucci, M. Chuan, C. Massagrande, P. Vinetti, M. Mattivi, R. Lombardi, and A. Massa, “Co-design of unconventional array architectures and antenna elements for 5G base station," *IEEE Trans. Antennas Propag.*, vol. 65, no. 12, pp. 6752-6767, Dec. 2017.

[25] N. Anselmi, P. Rocca, M. Salucci, and A. Massa, “Irregular phased array tiling by means of analytic schemata-driven optimization," *IEEE Trans. Antennas Propag.*, vol. 65, no. 9, pp. 4495-4510, Sept. 2017.

[26] N. Anselmi, P. Rocca, M. Salucci, and A. Massa, “Optimization of excitation tolerances for robust beamforming in linear arrays" *IET Microwaves, Antennas & Propagation*, vol. 10, no. 2, pp. 208-214, 2016.

[27] P. Rocca, R. J. Mailloux, and G. Toso, “GA-Based optimization of irregular sub-array layouts for wideband phased arrays desig," *IEEE Antennas and Wireless Propag. Lett.*, vol. 14, pp. 131-134, 2015.

[28] P. Rocca, M. Donelli, G. Oliveri, F. Viani, and A. Massa, “Reconfigurable sum-difference pattern by means of parasitic elements for forward-looking monopulse radar," *IET Radar, Sonar & Navigation*, vol 7, no. 7, pp. 747-754, 2013.

[29] P. Rocca, L. Manica, and A. Massa, “Ant colony based hybrid approach for optimal compromise sum-difference patterns synthesis," *Microwave Opt. Technol. Lett.*, vol. 52, no. 1, pp. 128-132, Jan. 2010.

[30] P. Rocca, L. Manica, and A. Massa, “An improved excitation matching method based on an ant colony optimization for suboptimal-free clustering in sum-difference compromise synthesis," *IEEE Trans. Antennas Propag.*, vol. 57, no. 8, pp. 2297-2306, Aug. 2009.

[31] N. Anselmi, L. Poli, P. Rocca, and A. Massa, “Design of simplified array layouts for preliminary experimental testing and validation of large AESAs," *IEEE Trans. Antennas Propag.*, vol. 66, no. 12, pp. 6906-6920, Dec. 2018.

[32] M. Salucci, F. Robol, N. Anselmi, M. A. Hannan, P. Rocca, G. Oliveri, M. Donelli, and A. Massa, “S-Band spline-shaped aperture-stacked patch antenna for air traffic control applications," *IEEE Trans. Antennas Propag.*, vol. 66, no. 8, pp. 4292-4297, Aug. 2018.

[33] F. Viani, F. Robol, M. Salucci, and R. Azaro, “Automatic EMI filter design through particle swarm optimization," *IEEE Trans. Electromagnet. Compat.*, vol. 59, no. 4, pp. 1079-1094, Aug. 2017.